Small-Angle X-ray Scattering of Spider Dragline Silk

Z. Yang,[†] D. T. Grubb,*[,‡] and L. W. Jelinski[†]

Center for Advanced Technology in Biotechnology, 130 Biotechnology Building, and Department of Materials Science and Engineering, Cornell University, Ithaca, New York 14853

Received April 22, 1997; Revised Manuscript Received August 6, 1997[⊗]

ABSTRACT: As part of a general study of the structure of spider silk fibers, major ampullate gland silk fibers were collected from *Nephila clavipes* spiders, and SAXS patterns were obtained from loops of fibers under a variety of conditions. Two orders of lamellar reflection were seen, with a long spacing of 8.4 nm. This increased reversibly by 4% when the fiber was stretched by 10% and shrank to 5.8 nm when the fiber itself shrank 45% on wetting. A strong equatorial streak had a bimodal orientation distribution similar to that seen in NMR and WAXD. The sharper component had a lateral size scale (radius of gyration) of 2.5 nm and a misorientation of 10° FWHM, similar to the orientation of the crystals. The minimum breadth of the streak indicates that the scattering objects are 0.1 μm long. There is an isotropic central scattering, probably caused by voids. On wetting, the lamellar peaks became more intense; more dramatically, the equatorial scattering strengthens and extends to higher angles, almost halving the lateral size scale to 1.4 nm. An equatorial maximum appears at a spacing of 6 nm, indicating a degree of order in the fibrillar structure.

Introduction

Spider dragline silk is one of the strongest protein-based materials that Nature has made. Its tensile strength is 1 GPa, comparable to that of steel, and it also requires high energy to break. These properties have generated considerable interest in spider silk, especially in the dragline silk from *Nephila clavipes*, the golden orb weaver, whose silk is among the strongest.[1] The dragline of *N. clavipes* is thought to comprise two different proteins synthesized in the major ampullate glands. Recent data[2] suggest that the freshly synthesized protein in the gland has a molecular weight as large as 720 000, with a polydispersity of 1.03. The polydispersity is taken as evidence for the presence of two closely related proteins. Amino acid analysis shows that 42% of the silk protein is glycine and 25% is alanine. Xu and Lewis[3] isolated and cloned about 2 kilobases from the 3′ (carboxy) ends and determined part of the DNA sequence of the two *N. clavipes* major ampullate proteins. The corresponding amino acid sequence has repeating units of polyalanine regions sandwiched between glycine-rich sequences containing bulky residues such as glutamine, arginine, and tyrosine.

X-ray diffraction[4,5] and Fourier transform infrared measurements[6] show that the ordered phase of silk has an antiparallel β-sheet structure. The spacing between the sheets agrees with that of β-polyalanine, suggesting that the crystallites contain primarily alanine. In a semicrystalline model of spider dragline silk,[7] the polyalanine regions form β-sheet crystals in an amorphous matrix. Our previous work with nuclear magnetic resonance (NMR)[8,9] on spider dragline silk suggests that there are two populations of alanine residues: 37% are well-oriented (FWHM of 5°) with the backbone parallel to the fiber axis, and the other 63% are slightly oriented with a FWHM angular distribution of 75°. NMR[9] and WAXD[10] both suggest a three-phase model is appropriate for the spider silk fibers. There are the well-oriented crystals and the isotropic amorphous material; the third phase is weakly oriented and partially ordered. The fraction of material in the crystalline phase is below 15%, and the crystals are very small, 2 × 5 × 6 nm.[10]

Mechanical tests imply that the fiber consists of solid crystalline particles in a soft rubbery matrix of a less ordered phase,[11] but the predicted stiffness is too low at a solids content of only 15%,[12] so it may be that the intermediate phase is stiff in the dry fiber. When the fiber is extended, the orientation of the crystals increases in agreement with the prediction of affine deformation so that the crystals appear to be carried around in the softer matrix.[10]

In most crystalline polymer fibers, the small-angle X-ray scattering (SAXS) pattern contains arcs or spots which come from stacks of crystals oriented along the fiber direction. The spacing gives the periodicity of the (crystal + disordered material) in the stacks or fibrils. Electron microscopy shows such stacks of lamellar crystals in deformed material.[13,14] The meridional reflection is called the "lamellar peak", even if the crystals are much the same size in every direction. It gives information about the regions where there is a more-or-less regular sequence of crystals and less ordered regions of lower density along the fiber direction.

When polymers contain voids, the SAXS patterns show a strong central diffuse scattering. Many synthetic and natural fibers contain elongated voids that give rise to a central scattering streak perpendicular to the draw direction.[15] Many also have a fibrillar structure, where the lateral boundaries of the crystal stacks define long thin objects parallel to the fiber axis.[13,16] These boundaries can also contribute to an equatorial streak. (Scattering from fiber surfaces can also contribute.[17,18]) Since the SAXS scattering intensity from a feature is proportional to the square of the local density change, it is often assumed that voids dominate the central scattering, which is then called the "void streak". However, if the streak shows a complicated structure, either it is not dominated by voids or the voids are interacting with the internal structure. In either case, there is structural information in the equatorial streak.

[†] Center for Advanced Technology in Biotechnology.
[‡] Department of Materials Science and Engineering.
[⊗] Abstract published in *Advance ACS Abstracts,* December 1, 1997.

S0024-9297(97)00548-2 CCC: $14.00

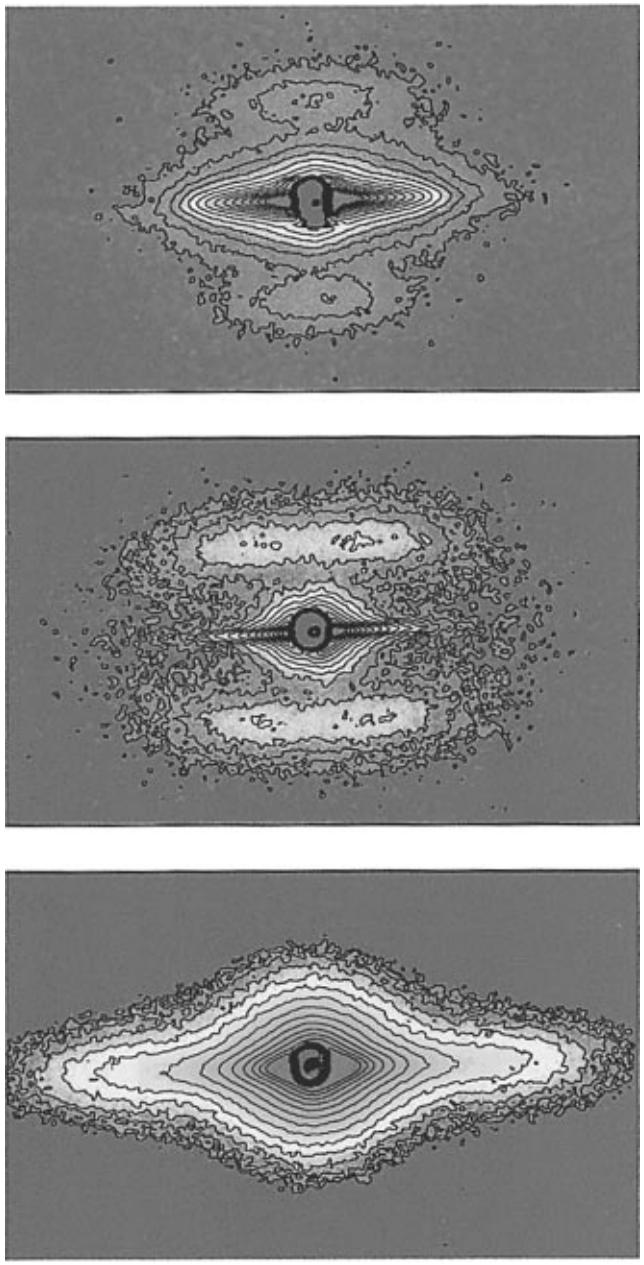

Figure 1. Fiber SAXS patterns. In Figures 1−4, the fiber direction is (near) vertical and the full horizontal scale of q is from −2.3 to +2.3 nm^{-1}. (a, top) From dry fibers of the dragline silk of *Nephila clavipes*. (b, middle) From nylon 6 fibers. The lamellar peaks are much stronger compared to the central scattering and much sharper than in a. (c, bottom) From silk fibers of the silkworm *Bombyx mori*. The lamellar peak is absent, and only a strong central scattering on the equator remains.

SAXS patterns of dry spider silk fibers have a strong equatorial streak and a weak reflection on the meridian (Figure 1a). Many synthetic fibers have a meridional peak that is much stronger compared to the equatorial streak (nylon 6, Figure 1b), but in other cases, for example, high-modulus fibers of polyethylene,[19,20] rigid-rod polymers,[21] or silk fibers from *Bombyx mori* (Figure 1c), the meridional peak may be very weak or absent. Thus, at the simplest qualitative level, the patterns are not unexpected and can be interpreted in terms of the standard fiber model.

Experimental Section

Fiber Samples. Spider dragline silk was collected from adult female *N. clavipes* obtained from central Florida. Silk production was initiated by manual stimulation at the spinneret, and the silk was collected[22] onto a piece of card taped around a cylinder, diameter 1 in. The draw rate was kept at 1.4 cm/s by turning the cylinder at ∼10 rpm. Two samples of dragline silk were collected. Each required 2 silkings of 2 spiders involving about 2000 turns in total. For deformation and diffraction, the sample loops were mounted over plated steel hooks clamped in the jaws of a simple tensile straining jig. The gauge length of the tensile sample was approximately half the circumference of the cylinder, and each tensile sample contained 4000 parallel fibers in 2 bundles. Sample A had an gauge length of 45.7 mm and weighed 2.11 mg; sample B had a gauge length of 43.7 mm and weighed 2.65 mg. Using 1.35 g/cm^3 as the density[1] gives mean fiber diameters of 3.3 and 3.6 μm, respectively. For diffraction, only one side of the loop was in the beam, so the sample cross-sectional areas were 0.017 and 0.022 mm^2. The International Silk Association kindly provided the *B. mori* silk used in these experiments. It was not degummed.

X-ray Measurements. SAXS measurements were made on the F1 beam line of the Cornell high-energy synchrotron source (CHESS). The F1 station provides a high-brightness beam converging to a focus. The convergence angles are 1 mrad in the horizontal plane and 0.3 mrad in the vertical plane. The source is tunable, and the peak intensity is $\sim 5 \times 10^{12}$ photons/(s·mm^2).[23] In this experiment, 13.63 keV photons ($\lambda = 0.091$ nm) and a collimator of diameter 0.1 mm were used. Exposure times were 60 s. The distance between sample and detector was 750 mm. To reduce air scatter, a chamber filled with helium replaced all but a few centimeters of the air path. It had a beryllium front window and a thin Mylar rear window. The beam stop was kept in contact with the rear window to reduce the effect of wide-angle scattering from the window material. The detector was a 1024 × 1024 CCD with a 50 × 50 mm sensitive area.

The tensile straining jig was mounted on a single axis rotation stage, which was itself mounted on a motorized $x-z$ stage. A microscope coupled to a TV camera allowed remote sample alignment, and background patterns were collected by moving the sample completely out of the beam. Sample extension was controlled manually with a micrometer screw. A load cell gave the tensile load, which was mainly used to ensure that the initial and unloaded states were under the minimum tension that gave a parallel fiber bundle. The experimental area was at low humidity, so to collect data from wet samples, a little cotton wool was used to wick distilled water from a dish onto the fiber bundle. Samples could be cooled with a chilled air flow cooler.

Analysis

The raw data files were first corrected for CCD background and distortion, and then the background patterns were subtracted, with correction for the changing incident flux. The pattern center and angle between the vertical and the fiber axis were found by collecting the intensity data around the circumference of a circle and searching (in a macro) for a center point that gave peaks of equal intensity 180° apart from the equatorial streak.

Meridional Peak. The standard method for the analysis of the meridional peak is to form the equivalent one-dimensional intensity $I_1(q_z)$

$$I_1 = \int_{-\infty}^{\infty} I(q_x,q_z) q_x \, \mathrm{d}q_x$$

and then perform correlation function analysis, following Vonk.[24] This type of analysis can give not only the long period but also the crystal thickness and information about the interface.[25] Unfortunately, this procedure does not work on our data. The problem is the relatively high intensity of the central diffuse scatter. Even in the meridional (z) direction, it overlaps the peak

(Figure 1), rapidly becomes much higher than the peak intensity, and dominates the computer fitting. The shape of the central diffuse scatter is not known, so it cannot be subtracted accurately from the peak. Indications that the procedure was not working were unreasonably large long periods and very small maximum and minimum values (0.005 instead of ~0.3) beyond the first zero in the correlation function plot. As a final check, the data range was limited to a region near the beam stop that excluded the entire meridional peak, and the same results were obtained.

We have had to rely on the simpler method of fitting the averaged meridional profile. A pair of Guinier scattering functions were used to fit the background central scattering and one or two Gaussian peaks for the reflections, giving the position, height, and width of the peaks. Here errors in background fitting are less important than in the correlation function analysis.

Equatorial Streak. Analysis of the equatorial streak is usually limited to its peak or integrated intensity as a function of q. Several theoretical expressions can be used to fit the data.[17,18,26] A common choice is the Guinier intensity distribution for isolated rodlike particles, $I \propto (1/q) \exp(-R_c^2 q^2/2)$, or a sum of such functions with different values of the radius of gyration of the cross section, R_c. Even though the Guinier approximation is strictly true only for the central part of the scattering from a dilute (uncorrelated) set of rods, it may be used to give an estimate of the lateral size of the scattering objects.[18,27] If the scattering objects are cylinders of diameter D, then $R_c = D/\sqrt{8}$.

The equatorial streak can be analyzed in more detail to derive the orientation distribution and size of the scattering objects in the fiber direction.[17,18,20,27,28] The idea is that the streak is broadened in the fiber axis direction both by misorientation and by the finite length of the scattering object. At larger angles, the orientation effect will dominate; at very small angles, the object size will dominate. Between these extremes, there is a combination of axial and angular smearing that must be dealt with by approximation or numerical simulation.

Results and Discussion

The results from two experimental runs are described here. In the first run, silk sample A1 was stretched 5.7% (A2) and then wetted while free of restraint so that it "supercontracted"[29] (A3). The shrunk fiber was partially dried (A4), restretched (A5), and relaxed (A6) while dry. In the second run, sample B1 was chilled to −32 °C (B2) and then gradually stretched to 10% strain (B3−B8). It was unloaded (B9), warmed up (B10), and restretched at room temperature to 12% (B11, B12). It was then wetted under tension (B13), allowed to relax while wet (B14, B15), and finally dried in the relaxed state (B16).

A general view of the whole pattern is important, though at present it can only be in qualitative terms. The images in Figures 1−4 are 340 × 320 pixels in size. They are obtained by averaging 3 × 3 pixel blocks in the original data and then low-pass filtering, clipping to remove distracting noise in the outer parts of the image, and finally taking the logarithm of the intensity to compress the dynamic range. They extend to $q \approx \pi(330 \times 0.15)/(750 \times 0.091) = 2.3$ nm^{-1}.

Figure 1a shows the original dry fiber (sample B1); there is a sharply defined narrow inner part to the equatorial streak, and the lamellar peaks are quite broad and not well separated from the central scatter.

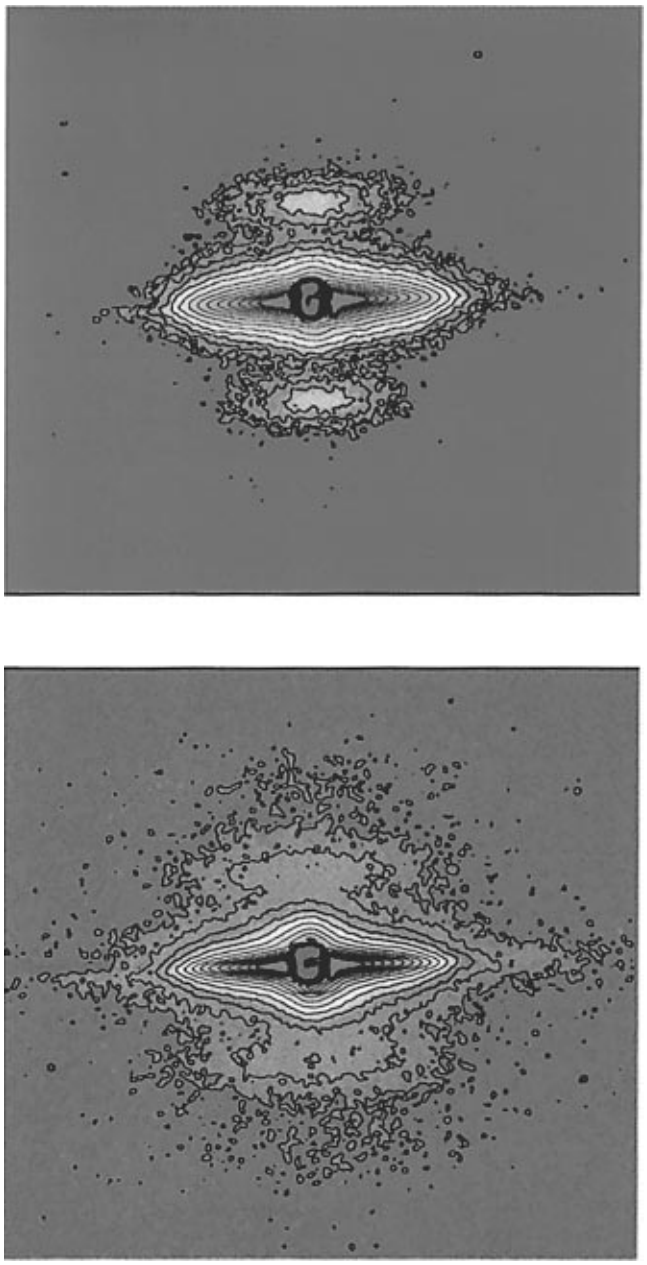

Figure 2. SAXS patterns of spider silk which has been stretched 10% at −32 °C and then relaxed, returned to room temperature, and redrawn. (a, top) Relaxed and at room temperature. This is essentially identical to Figure 1a and shows that the changes on extension are fully reversible. (b, bottom) At 12% extension. The narrow inner part of the equatorial streak is more distinct, and there is an additional isotropic scatter at the center. The shape and lateral extent of the lamellar peak is not changed.

When the sample is chilled to −32 °C, there is little visible change in the pattern. Drawing the sample to 10% extension at −32 °C has no permanent effect. Figure 2a, obtained after loading and relaxing (sample B10), is essentially identical to Figure 1a. Stretching once again at room temperature has the same effects as stretching at −32 °C. It makes the narrow inner part of the equatorial streak seem even more distinct, Figure 2b, sample B12, and there is an additional isotropic scatter at the center. The lamellar peak is less distinct, with no clear minimum on the meridian, at least in part due to the increased central scatter, but the shape and lateral extent of the lamellar peak is not changed.

These reversible changes are small compared to the irreversible changes that occur on wetting. Figure 3a,

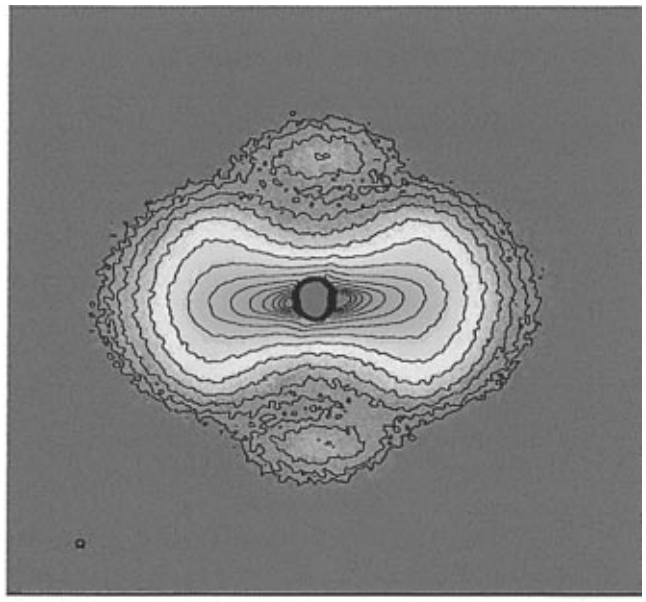

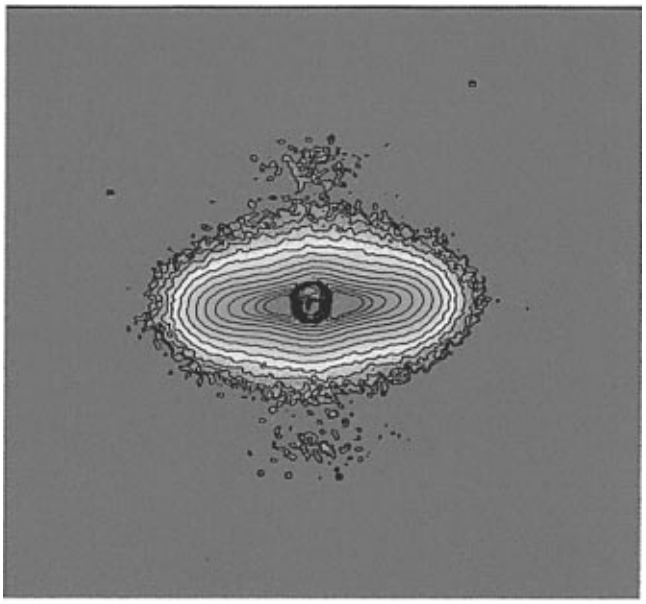

Figure 3. SAXS patterns of spider silk wetted and "supercontracted". (a, top) From sample A3, wet and 55% of its original length. New strong scattering appears on the equator. (b, bottom) After allowing the sample to dry. The extra scattering on the equator has disappeared.

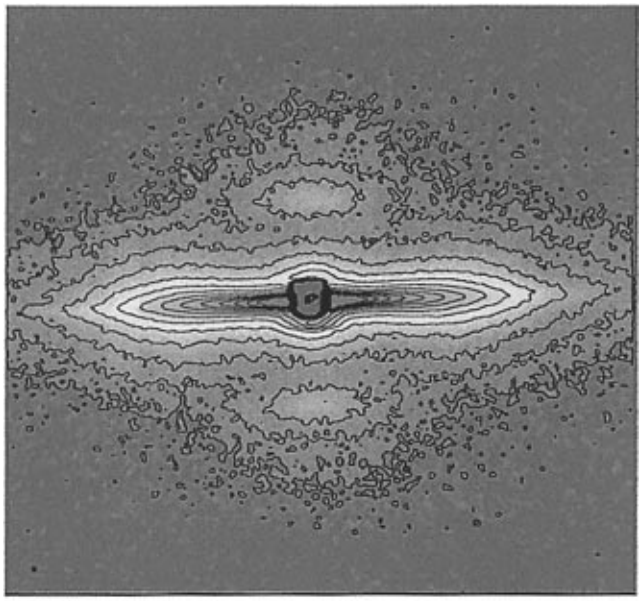

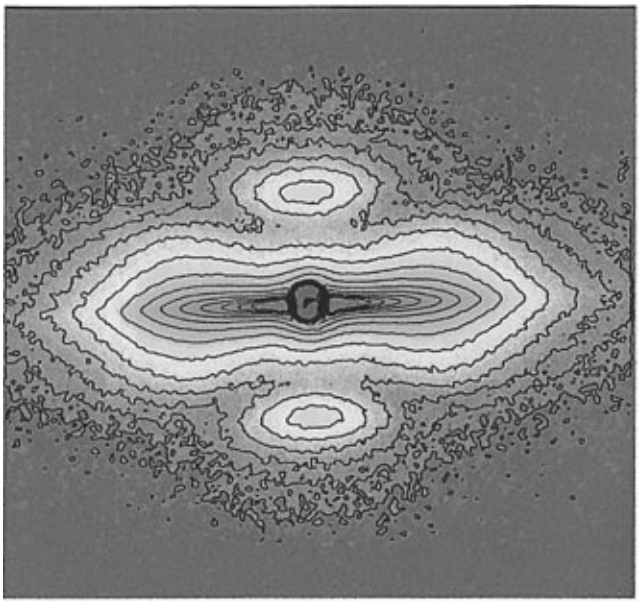

Figure 4. SAXS patterns of spider silk wetted while kept stretched. (a, top) At full length. Compared to the dry fiber (Figure 2b), there is a reduced central isotropic scatter and a stronger extended equatorial streak. (b, bottom) On release. The fiber does not shrink very much, but the SAXS scattering increases and the equatorial scattering shows a weak peak.

sample A3, had been wetted under no constraint and shrank to 55% of its original length. The lamellar peak has clearly moved out to larger angles, and the central streak has become much less well-oriented. More startling is the strong reflection which appears on the equator. This is due to the water, because on drying it disappears, Figure 3b (sample A6). What is left is a poorly oriented central streak and a much weaker lamellar peak, hardly visible in the image.

The second sample was wetted while it was held in the stretched state. Samples released from constraint after wetting in the stretched state shrink by only a few percent of the original length. Figure 4a shows sample B13, obtained by wetting the sample whose pattern is shown in Figure 2b. The central isotropic scatter is reduced, making the lamellar peak seem more distinct. The equatorial streak is strengthened and extends out to higher angles. The orientation of the pattern is maintained. When the sample is relaxed, the SAXS pattern, Figure 4b, appears to show some loss of orientation, but this could be the effect of the increased intensity of the equatorial peaks. Comparing the peaks in Figures 3a, 4a, and 4b, the great changes in shape and apparent orientation in the equatorial scattering are not accompanied by much change in the shape of the lamellar peak.

Meridional Peaks. All the patterns have peaks on the meridian, so a long period can be obtained from meridional intensity. Reassurance that Bragg's law can be applied to the meridional reflection comes from the observation of a second-order peak in all the patterns obtained from fibers which had not been wetted. Figure 5 shows the meridional intensity profiles from some dry fibers and the fitted curves. The background curve from central scattering (dashed line) is the sum of two

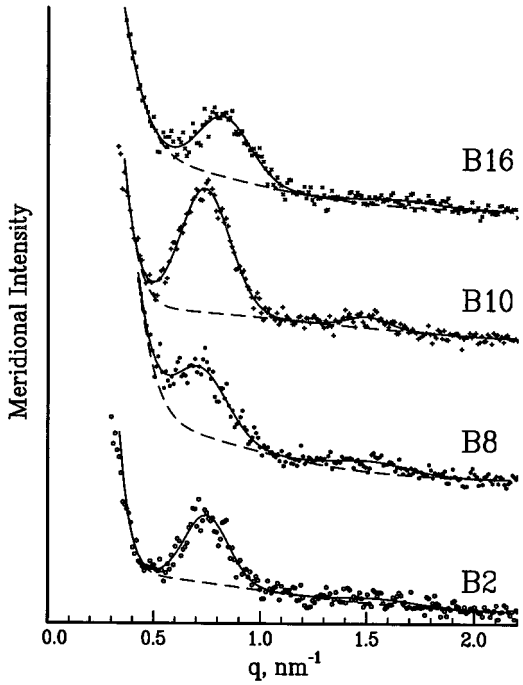

Figure 5. Intensity profile of the meridional scattering from dry samples. The intensity is averaged over a band 40 pixels wide (radially, 1 pixel = 0.0045 nm^{-1} Δq) and fitted to a sum of four Gaussian functions. Two are fixed at the center and fit the background scattering; two fit the lamellar peaks. B2 is unstretched, B8 stretched to 10.4%, and B10 relaxed. B16 has been wetted at constant length, allowed to relax, and then dried.

Gaussian functions, and the fit is usually good for a wider intensity range nearer the origin. The two peaks, clearest in B10, are well fitted by Gaussians of similar width, and the ratio of their positions is very close to 2.

The lowest curve in Figure 5 is from an unstretched fiber, B2. On stretching, B8, the peak moves slightly inward and the central scattering increases. A visible result is the more asymmetric appearance of the lamellar peak at higher strains, although the peak itself, from curve fitting, has the same shape and width. When the load is removed, B10, the fiber returns to almost the original length, and the scattering also returns to the original form. The fourth curve in Figure 5 is the meridional intensity from sample B16. The sample is then dry and only slightly (2%) shorter than it was for B10, but it has been exposed to water. The water has caused the lamellar spacing to decrease by 10%, and the shape of the central scattering is quite different. A weak and broad second-order peak is just detectable.

Changes in the SAXS lamellar peak caused by reversible deformation have been studied for a long time.[30−33] The macroscopic fiber strain ϵ is compared to the small-angle X-ray strain ϵ_d = (change in long period/original long period). In the "typical fiber structure" of polyethylene or nylon, $\epsilon \cong \epsilon_d$,[30] a homogeneous deformation expected since the fiber is almost entirely composed of the lamellar stacks. With a more closely controlled microstructure produced by drawing and rolling, the details of the deformation can be derived from the SAXS pattern.[31] Ginzburg and Tuichev[33] review studies of a wide range of polymers, where $\epsilon > \epsilon_d$, $\epsilon = \epsilon_d$, and $\epsilon < \epsilon_d$ are all seen and related to previous processing and thermal history. Generally, $\epsilon > \epsilon_d$ is associated with deformation by fibril slip and $\epsilon < \epsilon_d$ to unspecified inhomogeneity of deformation. The lamellar peaks generally weaken and become broader when the sample is in tension.

Table 1. SAXS Data

sample		lamellar reflections		equatorial streak angular width FWHM, deg	
name	extension l/l_0	long spacing, nm	spacing ratio 1st:2nd order	pk_1	pk_2
A1	1.0	8.34	2.17	(16.6 ± 0.4)	(40 ± 3)
A2	1.057	8.28	1.98	9.5 ± 0.2	29 ± 1
A3	0.55	5.86		23.7 ± 0.7	
A4	0.55	5.80		23.7 ± 0.9	
A5	0.64	5.48		12.0 ± 0.8	30 ± 2
A6	0.59	5.82		17.1 ± 0.3	37.7 ± 0.8
B1	1.0	8.48	2.06	7.1 ± 0.3	22.4 ± 0.8
B2	1.0	8.39	2.10	7.4 ± 0.7	22 ± 1.6
B3	1.013	8.48	2.09	6.2 ± 0.1	20.5 ± 0.7
B4	1.026	8.54	2.12	5.6 ± 0.1	19.3 ± 0.5
B5	1.039	8.52	2.11	5.4 ± 0.1	19.7 ± 0.5
B6	1.052	8.52	2.08	5.5 ± 0.15	19.4 ± 0.5
B7	1.09	8.73	2.13	5.5 ± 0.15	19.8 ± 0.5
B8	1.104	8.75	2.12	5.5 ± 0.2	19.6 ± 0.7
B9	1.0	8.55	2.18	7.7 ± 2	22 ± 4
B10	1.0	8.49	2.03	6.5 ± 0.3	21.2 ± 0.9
B11	1.08	8.73	2.03	4.8 ± 0.1	18.0 ± 0.3
B12	1.12	8.75	1.97	4.9 ± 0.3	18.1 ± 0.6
B13	1.12	8.03	1.80	5.2 ± 0.2	18 ± 1
B14	1.05	7.81		6.4 ± 0.5	
B15	0.98	7.37		7.2 ± 0.7	
B16	0.98	7.59	1.99	5.7 ± 0.5	21.7 ± 1.7

Table 1 shows the lamellar long period for all samples. No change in the width of the primary lamellar peak could be detected; it remained at a FWHM of $\Delta q = 0.27 \pm 0.02$ nm^{-1}. The average long spacing is 8.4 ± 0.1 nm for the dry fibers, and the average ratio of positions of the two peaks is 2.08 ± 0.06. On wetting the fibers, the peak becomes asymmetric and the second-order peak disappears. The change in spacing on wetting and changing the length of the wet specimens is shown in Figure 6a. The dry samples are shown as crosses and the wet ones as circles. Sample A was wetted under no constraint, the length fell to 0.55 of the original length, and the long spacing fell to 5.8 nm. Sample B was stretched by 11% while dry and then wetted at constant length when the long spacing fell to 7.9 ± 0.03 nm. When the wet fiber is allowed to relax, it shrinks, and the long spacing falls further. The effect is less than expected for homogeneous strain; the dashed line in Figure 6a has a slope of $\epsilon_d/\epsilon = 0.5$. On the scale of Figure 6a, the errors in the long spacing are about the size of the symbols.

The effect of tensile strain on dry fibers is shown in more detail in Figure 6b. The long spacing of the original fiber is shown as a cross. The series B2−B8 where the fiber is stretched while cold is shown as circles. The triangles show the results of a second elongation of the same sample, this time at room temperature. The dashed line is a linear fit to the initial stretching sequence. The slope is slightly less than in the case of the wet fibers, $\epsilon_d/\epsilon = 0.38$. The intensity of the lamellar peak falls on tensile deformation and increases when water is absorbed. The explanation of reduced deformation of crystal stacks in terms of interfibril slip[33] is more relevant to highly crystalline materials where we expect the fibrils to be closely packed. In spider silk with an overall crystallinity of about 15% and the lamellar stacks being apparently full of crystals, the fibrils will be well separated by disordered material. It is then natural to think of the fibrils as comparatively rigid elements in a composite, which will not be fully extended by the softer matrix.

The long period of 8.4 nm is difficult to reconcile with previous wide-angle X-ray results[10] which gave a mini-

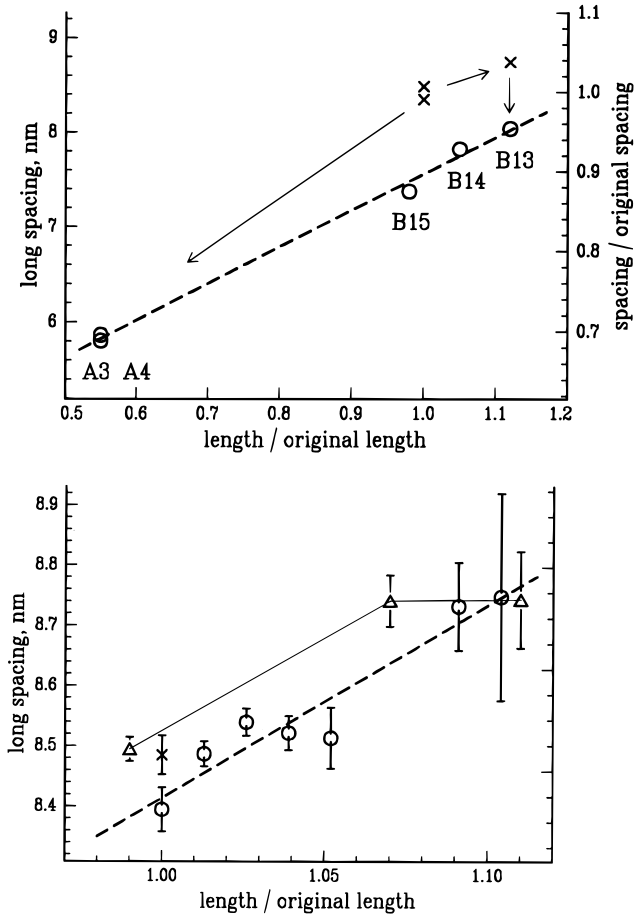

Figure 6. Effect of sample length changes on long spacing. (a, top) Wet fibers. The circles show the long spacings of wet fibers as a function of fiber strain, and the dashed line is a fit through these points. The arrows show how the wet fibers were obtained, and the crosses show the long spacing of the dry fibers. (b, bottom) Dry fibers. The circles are the fiber stretched at −32 °C, and the dashed line is the fit through these points. The cross is the original sample at room temperature. The open triangles are from restretching at room temperature (as in Figure 3).

mum crystal length along the [001] direction of 6−7 nm. When the fiber supercontracts and the long period falls to 5.8 nm, the problem is more obvious, for if the crystals are unaffected by wetting, they are apparently thicker than the long period, which is defined as (crystal thickness + amorphous thickness). One explanation could be the presence of a broad distribution of crystal sizes. The WAXD result gives a weight-average size, averaging over all the crystals, while a SAXS peak only comes from crystals of similar size in a regular stack. If the larger crystals are not regularly arranged, they do not contribute to the SAXS peak. As a simple example, consider a bimodal crystal thickness distribution where 70% of the crystals have thickness T and the rest $2T$. The RMS crystal thickness is $1.4T$. If the crystals are piled randomly into stacks, then one-third of the stack will consist of sequences of three or more small crystals, while only 3% consists of such sequences of large crystals. Let the amorphous layers be $0.4T$ thick, so the linear crystallinity of the stack is 76%. Modeling the diffraction expected from such a stack confirms the expectation that there is a clear peak very close to the long spacing of the thinner crystals, $1.4T$. In this case, the SAXS long spacing and the WAXD crystal size are the same.

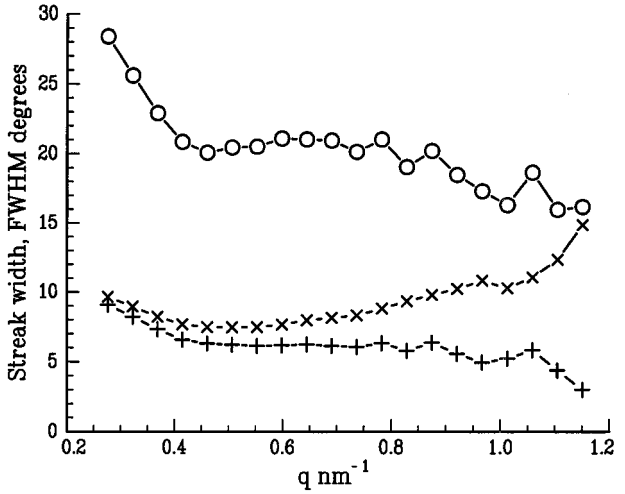

Figure 7. Angular width of the equatorial streak from sample B3, as a function of q. The upper and lower lines come from fitting the peak as the sum of two Gaussian functions, while the intermediate line (−x−) is from fitting as a single Pearson VII function.

A WAXD crystal size greater than the SAXS long period is not unique. It has been seen before in samples of high modulus polyethylene.[34, 35] A complex morphological explanation was given in that case, supported by mechanical modeling. This involved "intercrystalline bridges", molecules in the crystalline conformation that rigidly link adjacent crystals in a stack and make them appear as a single large crystal in WAXD.[35] This explanation is not appropriate to the silk case, since the amino acid sequence is known to contain only short crystallizable polyalanine segments.

Equatorial Streak. The broadening profile of the streak is a convolution of the axial size broadening, usually assumed to be Lorentzian, and the angular orientation broadening, usually assumed to be Gaussian. The data were scanned both at constant q and in strips parallel to the fiber axis, and the intensity profiles were fitted to a single Pearson VII function. The Pearson VII function has a power parameter p: when $p = 1$, the curve is Lorentzian; when p is large, the curve is Gaussian. The fit is good, but in most samples, it starts with high p at low q; p falls to < 1 as q increases. The simple expectation is the opposite, that p should start small and rise with q. A power parameter < 1 implies a sharp peak with long tails. A simple explanation is that the intensity is the sum of two peaks, one sharp and the other broad. The intensity was therefore refitted as the sum of two Gaussians.

Wet samples are fit with one Gaussian peak; for the rest, the best fit contains two peaks, with one peak 2−5 times wider than the other. (Sample A1 has asymmetric peaks; this may mean that the bundle was not completely taut. The measured angular width would then be partly due to misorientation of fibers in the bundle.) In dry samples, such as B3 shown in Figure 7, a narrow region of $0.5 < q < 0.9$ nm^{-1} has a constant value for the angular width of both peaks. Table 1 shows the angular widths measured in this region. The complex form of the streak indicates that it contains structural information. To emphasize this, Table 2 shows a summary of results on orientation in the dragline silk of *N. clavipes*, obtained by SAXS, WAXD, and NMR. Exact agreement is not expected, especially for NMR, which measures the orienatation of all alanine units, including those in amorphous domains. It is clear

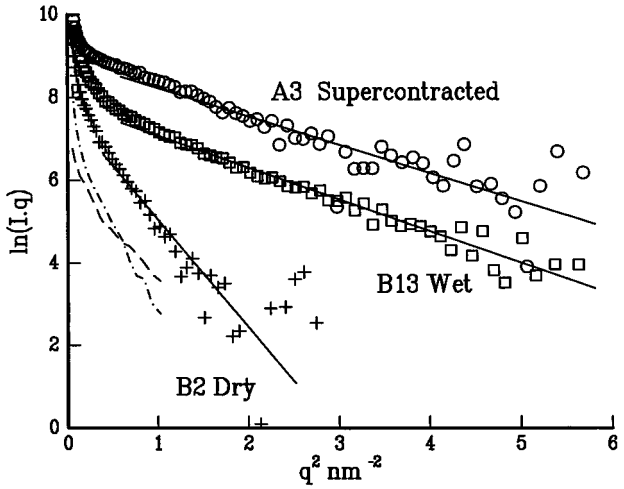

Figure 8. Intensities of the equatorial streak from samples B2 (dry), A3, and B13 (both wet), displaced vertically for clarity. All show a straight line when ln (Iq) is plotted against q^2. The slopes of the two wet samples are the same, although the sample lengths are very different. The dashed lines are the intensities of the two Gaussian functions fitted to the streak of sample B2, again displaced vertically.

Table 2. Summary of Orientation Measurements on the Dragline Silk of *N. clavipes*, Expressed as Approximate FHWM of Planes with Normals Perpendicular to the Chain Orientation, in Degrees

	in original state		
method	sharp peak	broad peak	in contracted state
SAXS equtr streak			
sample A	10−17	29−38	24
sample B	7	22	
WAX from ref 10	10	29	
WAX from ref 36	12	36	45
NMR from refs 8 and 9	2−12	75	

that all the X-ray data show a similar distribution of orientations. It would be surprising if small-angle and wide-angle scattering with such similarity did not arise from the same structures in some way. In WAXD, the well-oriented material is crystalline, and the poorly oriented material is amorphous or partially ordered.[10]

The upturn at small q in Figure 7 does not fit any of the functions that can be used to model the size-broadening effect.[20] It is therefore due to overlap from other central scattering. This scattering increases in intensity on extension and is reduced by wetting, so it comes from voids and perhaps surface effects at low angles.[17,18] It is more difficult to believe that the rest of the equatorial scattering comes from voids when it behaves so differently. Avoiding the central (void scattering) part of the curve, the angular width of the data at $q = 0.43$ nm^{-1} is 8°. This is a FWHM of $\Delta q = 0.048$ nm^{-1} in absolute terms, and using $L = 0.8/\Delta s = 1.6\pi/\Delta q$, the size of the scattering object in the fiber axis direction is at least 105 nm. A similar result for sample B, $\Delta q = 0.044 \pm 0.002$ nm^{-1}, gives a length of 115 nm.

Figure 8 shows the peak intensity of the equatorial streaks in the form of Guinier plots for rods, ln(Iq) vs q^2. B2 is given as an example of the dry fibers, which are all very similar. There is a reasonable straight line section and the usual upturn at low q. These data can be interpreted as due to a single set of rodlike objects, of transverse radius of gyration $R_c = 2.6$ nm. Combining data from all the dry samples gives $R_c = 2.55 \pm 0.07$ nm. For cylinders, this would mean a diameter of 7.2 ± 0.2 nm and thus an aspect ratio of 16.

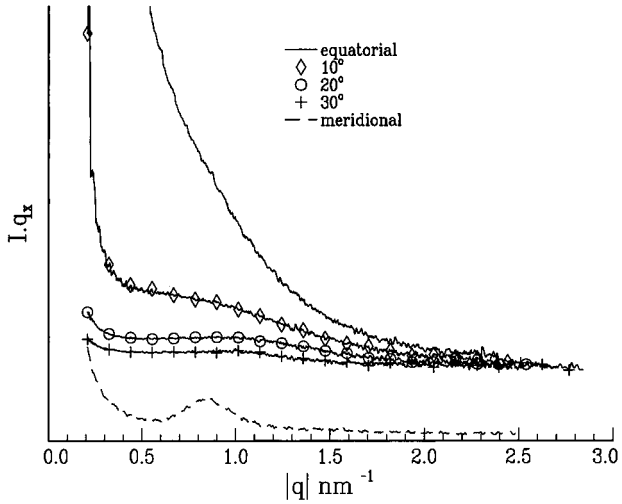

Figure 9. Fiber Lorentz-corrected intensity from sample B13. The equatorial streak shows no maximum, but there is a clear broad peak between 0.5 and 1.5 nm^{-1} in the off-axis intensities. The meridional intensity, vertically displaced, is shown for comparison with the lamellar peak.

There is a very significant change on wetting the fiber, as shown in Figure 8. The intensity falls off much more slowly with q. This is due to wetting and not to sample deformation since the new slope is the same for the fiber wetted at constant length (B13−B15) and for the supercontracted fiber A3. Combining data from all the wet samples gives $R_c = 1.43 \pm 0.06$ nm (cylinders of ∼4-nm diameter). If the scattering in the dry sample is due to the difference in density between crystalline regions and less well-ordered regions, then it is natural to expect an increase in intensity on wetting (scattering from voids should decrease). The water will more easily enter the disordered material and will reduce its density further. However, one would also expect that the size scale should increase on swelling, whereas here it decreases by almost a factor of 2. This lateral size reduction cannot be explained by distortion of previously existing structure. It implies either that the fibril structure is split into narrower units or that a totally new structure appears with stronger scattering that hides the original structure. Since the silk protein is not chemically homogeneous, this new structure might be due to segregation of regions of more hydrophilic residues which attract more water.

Figures 3 and 4 clearly show a peak on the equator in the wetted samples, but there is little indication of this in Figure 8. Figure 9 shows Lorentz-corrected intensity (Iq_x) as a function of $|q|$ in different directions for sample B15. There are clear peaks at $q \approx 1$ nm^{-1} in the scans taken at 10, 20, and 30° to the equator. The intensity on the equator itself is so great that a peak of similar height could be present and not visible. The FWHM of the peak is about 0.7 nm^{-1}. A meridional scan is included for comparison, and it can be seen that the lamellar peak is at a similar but slightly smaller angle and is much sharper. A new periodicity is another clear indication that a previously invisible structure is appearing when water is absorbed.

A strong peak on the equator of oriented of fibrous polymers has been seen in other natural and synthetic polymers.[37,38] When fitting normal two-point fiber SAXS patterns with elliptical coordinates, it was found necessary to add weak peaks on the equator, peaks that

were not clearly visible in the raw data.[39] These peaks were assigned to regularities in the arrangement of the fibrils. We can apply this explanation to spider silk, but the data in Figure 9 show that the equatorial peak is spread out in the fiber axis direction while the equatorial streak remains sharp. The objects that are regularly spaced are very poorly aligned or very short. If the water-induced structure comes from fibrils, it seems that the less well-oriented fibrils are broken up into short segments on swelling in water and that this breakup allows some lateral regularity.

Conclusions

The biological samples show variability. Samples A and B had significantly different degrees of orientation, although they were collected under the same conditions and stored in the same way. It is apparent that in the future, comparative wide-angle and small-angle diffraction should be obtained from the same specimen, preferably at the same time.

We find that the lamellar structure of the dragline silk of *N. clavipes* deforms less than the fiber does. Its strain is 38% of the fiber strain when dry fibers are extended and 50% of the fiber strain when wet fibers shrink. This might be expected for low-crystallinity material where lamellar stacks are embedded in softer material. Unexpectedly, in the supercontracted state, the periodicity is 5.8 nm, less than the minimum crystal size derived from wide-angle X-ray diffraction.[10] This discrepancy can be explained by assuming a wide range of crystal sizes.

Detailed analysis of the equatorial streak shows that it contains information about the structure of the fiber. The minimum observed width of the equatorial streak in the fiber axis direction implies that there are diffracting objects 0.1 μm long in fiber direction, and its shape shows that the aspect ratio of these objects is over 10:1. The orientation distribution of these objects is bimodal and similar to that found for the equatorial WAXD reflections. This indicates that the two distributions of crystals are located separately, in groups of their own kind, as was implied in the schematic model derived from NMR data.[18]

Complex changes occur when the fibers are wetted that are not fully understood; more work needs to be done in this area. We find that when the fibers are wetted, the lateral size scale changes from 2.5 to 1.5 nm. A new broad peak appears on the equator at $q \approx 1\ nm^{-1}$, corresponding to a spacing of 6 nm. These changes are not related to shrinkage and reverse when the fiber is dried.

Acknowledgment. We thank David Hijirida for collecting silk from spiders and Carl Michal, Tak Yan Tse, and Oskar Liivak for their help in the care and feeding of spiders and in specimen preparation. Dr. N. S. Murthy and David Jackrel helped in setting up the SAXS experiment and with the tensile apparatus. Data collection would not have been possible without the help of CHESS and MacCHESS staff. Dr. Benjamin Hsiao gave advice on correlation analysis which was highly appreciated. We also thank the National Science Foundation (MCB-9601018) and the National Textile Council for their financial support.

References and Notes

(1) Zemlin, J. C. Technical Report 69-29-CM (AD684333); US Army Natick Laboratories, Natick, MA, 1968.
(2) Jackson, C.; O'Brien, J. P. *Macromolecules* **1995**, *28*, 5975.
(3) Xu, M.; Lewis, R. V. *Proc. Natl. Acad. Sci. U. S. A.* **1990**, *87*, 7120.
(4) Warwicker, J. O. *J. Mol. Biol.* **1960**, *2*, 350.
(5) Becker, M. A.; Mahoney, D. V.; Lenhert, P. G.; Eby, R. K.; Kaplan, D.; Adams, W. W. In *Silk Polymer: Materials Science and Biotechnology*, ACS Symposium Series 544; American Chemical Society 1994 p185.
(6) Dong, Z.; Lewis, R. V.; Middaugh, C. R. *Arch. Biochem. Biophys.* **1991**, *284*, 53.
(7) Lewis, R. V. *Acc. Chem. Res.* **1992**, *25*, 395.
(8) Simmons, A. H.; Ray, E.; Jelinski, L. W. *Macromolecules* **1994**, *27*, 5235.
(9) Simmons, A. H.; Ray, E.; Jelinksi, L. W. *Science* **1996**, *271*, 84.
(10) Grubb, D. T.; Jelinski, L. W. *Macromolecules* **1997**, *30*, 2860.
(11) Gosline, J. M.; Denny, M. W.; DeMont, M. E. *Nature* **1984**, *309*, 551.
(12) Termonia, Y. *Macromolecules* **1994**, *27*, 7378.
(13) Odell, J. A.; Grubb, D. T.; Keller, A. *Polymer* **1987**, *19*, 617.
(14) Yang, D. C.; Thomas, E. L. *J. Mater. Sci.* **1984**, *19*, 2098.
(15) Statton, W. O. *J. Polym. Sci.* **1962**, *58*, 205.
(16) Schaper, A.; Zenke, D.; Schulz, E.; Hirte, R. Taege, M. *Phys. Stat. Sol. (A)* **1989**, *116* (1), 179.
(17) Perret, R.; Ruland, W. *J. Appl. Crystallgr.* **1970**, *3*, 525.
(18) Gupta, A.; Harrison, I. R.; Lahijani, J. *J. Appl. Crystallgr.* **1994**, *27*, 627.
(19) Hoogsteen, W.; Pennings, A. J.; ten Brinke, G. *Colloid Polym. Sci.* **1990**, *268*, 245.
(20) Grubb, D. T.; Prasad, K. *Macromolecules* **1992**, *25*, 4575.
(21) Kumar, S.; Warner, S.; Grubb, D. T.; Adams, W. W. *Polymer* **1993**, *35*, 5409.
(22) Work, R. W.; Emerson, P. D. *J. Arachnol.* **1982**, *10*, 1.
(23) For more details, see http://www.chess.cornell.edu/Facility/F1_station.html.
(24) Balta-Calleja, F. J.; Vonk, C. G. *X-ray Scattering of Synthetic Polymers (Polymer Science Library Vol 8)*; Elsevier: Amsterdam, New York, 1989..
(25) Verma, R. K.; Velikov, V.; Kander, R. G.; Marand, H.; Chu, B.; Hsiao, B. S. *Polymer* **1996**, *37*, 5357.
(26) Aerts, J. *J. Appl. Crystallgr.* **1991**, *24*, 709.
(27) Murthy, N. S.; Bednarczyk, C.; Moore, R. A. F.; Grubb, D. T. *J. Polym. Sci. B Polym. Phys.* **1996**, *34*, 821−835.
(28) Grubb, D. T.; Prasad, K.; Adams, W. W. *Polymer* **1991**, *32*, 1167.
(29) Work. R. W.; Morosoff, N. *Text. Res. J.* **1982**, *52*, 349.
(30) Ishikawa, K.; Miyaska, K.; Maeda, M.; Yamada, M. *J. Polym. Sci., A-2* **1969**, *7*, 1259.
(31) Keller, A.; Pope. D. P. *J. Mater. Sci.* **1971**, *6*, 453.
(32) Wu, W-L.; Zachmann, H. G.; Rickel, C. *Polymer Comm.* **1984**, *25*, 76.
(33) Ginzburg, B. M.; Tuichev, Sh. *J. Macromol. Sci.* **1992**, *B 31*, 291.
(34) Clements, J.; Jakeways, R.; Ward, I. M. *Polymer* **1978**, *19*, 639.
(35) Gibson, A. G.; Davies, G. R.; Ward, I. M. *Polymer* **1978**, *19*, 683.
(36) Grubb, D. T.; Jackrel, D.; Jelinski, L. W. To be published.
(37) Fraser, R. D. B.; MacRae, T. R. *J. Molec. Biol.* **1961**, *3*, 640.
(38) Seguela, R.; Rietsch, F. *Polym. Comm.* **1987**, *28*, 256.
(39) Murthy, N. S.; Zero, K.; Grubb, D. T. *Polymer* **1997**, *38*, 1021.

MA970548Z